Divergence of trafficking and polarization mechanisms for PIN auxin transporters during land plant evolution

Han Tang[1,5], Kuan-Ju Lu[2,5], YuZhou Zhang[3], You-Liang Cheng[4], Shih-Long Tu[4], and Jiří Friml[1]*

1. Institute of Science and Technology Austria (ISTA), Am Campus 1, 3400 Klosterneuburg, Austria
2. Graduate Institute of Biotechnology, National Chung Hsing University, No. 145, Xingda Rd., South Dist., Taichung 40227, Taiwan, R.O.C.
3. College of Life Sciences, Northwest A&F University, Shaanxi, Yangling, China.
4. Institute of Plant and Microbial Biology, Academia Sinica, 128 Sec. 2, Academia Rd, Nankang, Taipei 11529, Taiwan, R.O.C.

5. These authors contribute equally to this work.
* Correspondence: jiri.friml@ist.ac.at

The author responsible for distribution of materials integral to the findings presented in this article in accordance with the policy described in the Instructions for Authors (https://academic.oup.com/plcell) is: Jiri Friml (jiri.friml@ist.ac.at, +43 2243 9000 5401)).

Running title: Evolution of PIN trafficking and polarization

Abstract

The phytohormone auxin and its directional transport through tissues play a fundamental role in development of higher plants. This polar auxin transport predominantly relies on PIN-FORMED (PIN) auxin exporters. Hence, PIN polarization is crucial for development, but its evolution during the rise of morphological complexity in land plants remains unclear. Here, we performed a cross-species investigation by observing the trafficking and localization of endogenous and xenologous PINs in two bryophytes, *Physcomitrium patens* and *Marchantia polymorpha*, and in the flowering plant *Arabidopsis thaliana.* We confirmed that the GFP fusion did not compromise the auxin export function of all examined PINs by using radioactive auxin export assay and by observing the phenotypic changes in transgenic bryophytes. Endogenous PINs polarize to filamentous apices, while xenologous Arabidopsis PINs distribute symmetrically on the membrane in both bryophytes. In Arabidopsis root epidermis, bryophytic PINs show no defined polarity. Pharmacological interference revealed a strong cytoskeleton dependence of bryophytic but not Arabidopsis PIN polarization. The divergence of PIN polarization and trafficking is also observed within the bryophyte clade and between tissues in individual species. These results collectively reveal a divergence of PIN trafficking and polarity mechanisms throughout land plant evolution and a co-evolution of PIN sequence-based and cell-based polarity mechanisms.

Key words: Arabidopsis, evolution, Marchantia, Physcomitrium, PINs, polarization, protein trafficking

Introduction

Auxin is a crucial regulator of polarity and morphogenesis in land plants (Kato et al., 2018; Leyser, 2018; Mockaitis and Estelle, 2008; Smit and Weijers, 2015; Yu et al., 2022). The auxin gradients and local maxima within tissues coordinate a broad spectrum of plant development, ranging from embryogenesis to organ formation and tropisms (Friml, 2021; Vanneste and Friml, 2009). The establishment of the auxin gradient relies dominantly on directional auxin transport driven by the efflux carriers, PIN-FORMEDs (PINs). In different tissues, specific PINs are polarized at different plasma membrane (PM) domains, thus directly driving the directionality of auxin flow (Adamowski and Friml, 2015). Therefore, given the essential impact of auxin flow in various developmental processes, the function and polarization of PIN proteins are crucial for maintaining the correct pattern of plant growth and patterning (Sauer and Kleine-Vehn, 2019).

PINs are found in all land plants and can be traced back to charophytic green algae (Skokan et al., 2019; Viaene et al., 2013). The functional conservation of PINs in the auxin transport has also been demonstrated by exogenously expressing PINs from the green algae *Klebsormidium flaccidum* (*K. flaccidum*), the moss *Physcomitrium patens* (*P. patens*), and the angiosperm *Arabidopsis thaliana* in transgenic plants and in heterologous systems (Skokan et al., 2019; Zourelidou et al., 2014). Additionally, when xenologous PINs from charophytes or Arabidopsis are overexpressed in *P. patens*, the transgenic plants show growth inhibition that resembles auxin deprivation phenotypes (Lavy et al., 2016; Skokan et al., 2019; Tao and Estelle, 2018; Viaene et al., 2014). Therefore, these observations support the idea that PIN-mediated polar auxin transport may govern plant development since the emergence of land plants.

PIN polarity regulations have been extensively investigated in the angiosperm Arabidopsis. Canonical PINs, featuring a long central hydrophilic loop (HL) between two transmembrane domains, are delivered via the ER-Golgi vesicle trafficking pathway to the plasma membrane (PM). De-polymerization of actin filaments induces the accumulation of PIN-labelled small intracellular puncta near the PM, but with no apparent PIN polarity defect (Geldner et al., 2001; Glanc et al., 2018; 2019). Microtubules are involved in the cytokinetic trafficking of PINs, but are not required for the polarity establishment or maintenance at the PM of non-dividing cells (Geldner et al., 2001; Glanc et al., 2019; Kleine-Vehn et al., 2008b). Notably, the disruption of both

99 cytoskeletal networks delays but does not abolish AtPIN2 polarization in Arabidopsis
100 epidermal cells (Glanc et al., 2019). This suggests that the cytoskeletal networks are
101 involved, but not strictly essential for PIN polar trafficking, while other mechanisms
102 contribute to the PIN polar localization. PINs are known to undergo constitutive cycles
103 of endocytosis and recycling, which is modulated by auxin itself (Narasimhan et al.,
104 2021; Narasimhan et al., 2020); this process is essential for their polar distribution
105 (Doyle et al., 2015; Kleine-Vehn et al., 2011).
106 The Phosphorylation of specific sites within the HL region has been
107 demonstrated to be a critical determinant for PINs' apical-basal polarization in
108 Arabidopsis epidermis. A serine/threonine kinase, PINOID (PID), phosphorylates
109 specific sites on AtPIN2 and leads to its apical localization (Friml et al., 2004). In
110 contrast, when phosphatase 2A (PP2A) de-phosphorylates AtPIN2, which counteracts
111 the PID-dependent phosphorylation, and thus guides the delivery of AtPIN2 to the
112 basal domain of epidermal cells (Michniewicz et al., 2007). The phosphorylation sites
113 targeted by different kinase families are crucial for polar localizations and functions of
114 PINs, and most sites are highly conserved within Arabidopsis canonical PINs
115 (Zwiewka et al., 2019). Since PINs are present in all land plants, one can hypothesize
116 that the phosphorylation-based polarity regulation may have been established since
117 the emergence of early land plants. However, it has never been clarified whether these
118 phosphorylation sites are evolutionary conserved in early land plants.
119 The PIN polarization has been observed in the early-divergent moss, *P. patens*,
120 which grows as filamentous protonemata, and its endogenous PpPINA-GFP shows a
121 polar localization at the tip of protonema cells (Bennett et al., 2014; Viaene et al., 2014).
122 However, the polar localization of PpPINA-GFP is not robust in other species. When
123 PpPINA-GFP is expressed in Arabidopsis root epidermal cells, where AtPIN2-GFP
124 presents a clear apical localization, PpPINA-GFP is mislocalized at both basal and
125 apical sites (Zhang et al., 2019). Furthermore, PINs from the liverwort, *Marchantia*
126 *polymorpha* (*M. polymorpha*), and from the green algae, *K. flaccidum*, are also
127 mislocalized in root epidermal cells of Arabidopsis (Zhang et al., 2019). These
128 distinctive PIN localizations in different species suggest that mechanisms for PINs
129 trafficking and polarization may have diversified after the emergence of land plants.
130 Despite the profound significance of PIN polarization and the resulting directional
131 auxin transport for land plant development, PIN trafficking and polarization
132 mechanisms are mainly derived from the angiosperm model *Arabidopsis thaliana*.

133 Here we investigated PIN trafficking/polarization mechanisms from an
134 evolutionary perspective. We show that canonical PINs from bryophytes *P. patens*, *M.*
135 *polymorpha,* and Arabidopsis present high conservation in their transmembrane
136 domains and phosphorylation sites. Endogenous PIN-GFPs show different localization
137 patterns in various developmental contexts, suggesting tissue-specific PIN
138 polarization mechanisms. Cross-species investigation revealed that xenologous PINs
139 can traffic to the PM but fail to enrich at the polar domains revealing species-specific
140 mechanisms for PIN polarization. This notion was further verified by different
141 dependency of cytoskeletons for the polarization of Arabidopsis PINs and bryophytic
142 PINs. Overall, our results highlight that PINs trafficking and polarization mechanisms
143 underwent complex evolution during the gradual rise of morphological complexity in
144 land plants.
145
146 **Results**
147 **Phosphorylation sites are highly conserved between bryophytic and**
148 **Arabidopsis PINs**
149 To dissect the conservation between bryophytic and Arabidopsis PINs, we first
150 performed a phylogenetic analysis. The coding sequence of the single canonical PIN,
151 MpPINZ, from *M. polymorpha*, three canonical PINs, PpPINA-PpPINC, from *P. patens*,
152 and five canonical PINs, AtPIN1-AtPIN4 and AtPIN7, from Arabidopsis were subjected
153 to MEGA X program (Kumar et al., 2018) for the phylogenetic study. Bryophytic PINs
154 are categorized in one group, and the MpPINZ is closer to Arabidopsis PINs than
155 PpPINs are (Figure 1A). Arabidopsis AtPIN1 and AtPIN2 were identified with clear
156 polarity at the PM that plays crucial role in embryogenesis, organ formation, and tropic
157 growth (Krecek et al., 2009; Omelyanchuk et al., 2016). The phylogenetic tree showed
158 that both AtPIN1 and AtPIN2 are equally close to bryophytic PINs, while AtPIN2 was
159 extensively investigated for its polarization in roots (Abas et al., 2006; Glanc et al.,
160 2018; Kleine-Vehn et al., 2008a), thus we first picked AtPIN2 as our reference for
161 further alignment analyses. The identity index of coding amino acid sequences
162 showed that full-length AtPIN2 has around 50% identity with each bryophytic PIN
163 (Figure 1B). Since the transmembrane domains show a high similarity between all
164 examined PINs, we suspected that central HLs are more divergent. Surprisingly, the
165 identity index for only the HL region of AtPIN2 presented over 40% identity with

166 MpPINZ (45%), PpPINA (42%), and PpPINB (43%) (Figure 1B). The identity index of
167 full-length AtPIN1 and HLs showed similar results as AtPIN2 (Supplemental Figure 1).
168 The overview of coding sequences for all examined PINs revealed highly
169 conserved transmembrane domains at N-terminus and C-terminus, connected by a
170 less conserved HL region (Figure 1C). Because the polarization of AtPIN2 is tightly
171 associated with its phosphorylation status on the HL, we used AtPIN2 as a reference
172 to search for and highlight these experimental-identified phosphorylation sites
173 (Barbosa et al., 2018; Sukumar et al., 2009; Zhang et al., 2010). Comparing to
174 transmembrane domains, despite of a relatively lower conservation in their HLs, the
175 four identified phosphorylation sites are fully conserved between Arabidopsis PINs and
176 bryophytic PINs (Figure 1D), which suggests that the PIN phosphorylation might be
177 evolutionarily conserved for the regulation of their intracellular localization.
178
179 **The hydrophilic loops in AtPIN2, PpPINA, and MpPINZ are less conserved**
180 To dissect how conserved between Arabidopsis PINs and bryophytic PINs is in their
181 protein structures, we next performed structural prediction and alignment. Structures
182 predicted by the Alphafold2 program resemble newly resolved structures of AtPIN1
183 and AtPIN8 (Supplemental Figure 2) (Jumper et al., 2021; Ung et al., 2022; Yang et
184 al., 2022), supporting that the structure prediction is reliable. Therefore, to compare
185 the structures of well-investigated polarized AtPINs, we predicted the structures of
186 AtPIN1 and AtPIN2 by Alphafold2 and aligned their predicted structures in ChimeraX
187 (Jumper et al., 2021; Pettersen et al., 2021). The structural conservation was
188 presented in almost perfect alignment of transmembrane domains while their HL
189 regions showed similar patterns (Figure 2A, close arrowheads) with two extra random
190 loops in AtPIN2 (Figure 2A, open arrowheads). We next aligned the structure of AtPIN2
191 with PpPINA and MpPINZ. The transmembrane domains are highly conserved with
192 nearly perfect alignments, but the HLs are less conserved that only one loop showed
193 partial similarity (Figure 2B, close arrowheads). Note that to reveal the conservation
194 and phosphorylation sites clearly, the orientation of protein structures presented in
195 Figure 2A and 2B-E were rotated in different angles. In general, bryophytic PINs
196 possess loosen and larger loops compared to AtPIN2 (Figure 2B-2E). The predicted
197 structures were shown individually with the annotated phosphorylation sites that are
198 indicated in Figure 1D (Figure 2C-2E). The structural conservations in transmembrane
199 domains imply that ancestry bryophytic PINs may traffic to the PM through the same

200 delivery pathways as Arabidopsis PINs, whereas the loosen loops with conserved
201 phosphorylation sites suggest a deviation from conserved regulation for their
202 polarization.
203
204 **GFP-fused PIN proteins possess auxin export activity**
205 The sequence and structural analyses between Arabidopsis PINs and bryophytic PINs
206 revealed high conservation in sequence, phosphorylation sites, and structures of
207 transmembrane domains. Thus, we next would like to investigate whether bryophytic
208 PINs are delivered to the PM with polar domain enrichment as Arabidopsis PINs. To
209 achieve this, we first generated PINs with GFP-fused into an equivalent position of
210 AtPIN1, AtPIN2, PpPINA, and MpPINZ as shown in Figure 3A (Zhang et al., 2019). To
211 verify the auxin export function of these GFP-fused PINs, we subcloned each GFP-
212 fused *PIN* gene into a moss vector, where each *PIN-GFP* gene was driven by an
213 inducible *XVE* promoter (Kubota et al., 2013). We generated transgenic moss plants
214 carrying different *XVE::PIN-GFPs* separately, and we used these transgenic lines to
215 perform the auxin export assay. In brief, the overexpression of *PIN-GFPs* were
216 induced for 3 days, followed by a radioactive auxin H^3-IAA treatment for 24 hours. The
217 radioactive tissues were then washed twice and were incubated in fresh growth
218 mediums for another 24 hrs. The culture medium was collected for H^3 scintillation
219 detection (Lewis and Muday, 2009). The wild-type moss plants were taken along as
220 an internal control to show the basal exportation of H^3-IAA by endogenous PpPINs. In
221 comparison to the wild-type, all examined PIN-GFP plants showed higher amount of
222 radioactive auxin in the culture medium, indicating their auxin export activities (Figure
223 3B).
224 Additionally, the function of PIN-GFPs was also confirmed in the growth
225 changes caused by *PIN-GFPs* overexpression in both *P. patens*. and *M. polymorpha*.
226 During early development, *P. patens* gradually transits its filamentous protonemata
227 from thicker/shorter chloronema cells with perpendicular division planes to
228 thinner/longer caulonema cells with oblique division planes (Rensing et al., 2020). In
229 the previous study, PpPINA, PpPINB, and PpPIND overexpression has been
230 demonstrated to inhibit the protonema transition (Viaene et al., 2014). Here we
231 showed that overexpression of *PpPINA-, AtPIN1-*, and *AtPIN2-GFP* led to similar
232 defects in this chloronema-caulonema transition with a shorter cell length of the
233 subapical cell and a smaller division angle (Figure 3C-3E). The wild-type *M.*

234 *polymorpha* has prostrate thalli; however, with the overexpression of either *MpPINZ-*
235 *GFP* or *AtPIN-GFPs*, the thallus grew more vertically, as apparent from the side view
236 (Figure 3F), phenocopying the auxin deficient phenotype (Kato et al., 2017). The
237 angles between the thallus and the horizontal agar were measured to quantify the
238 vertical growth (Figure 3G). The overexpression of *MpPINZ-GFP* caused the most
239 striking phenotype, but the overexpression of *AtPIN-GFPs* also resulted in a vertical
240 growth that showed significant differences from the wild-type. Our results show that all
241 PIN-GFPs can export auxin in the moss system and cause phenotypic changes in both
242 *P. patens* and *M. polymorpha* upon overexpression.
243
244 **Endogenous PINs present different localization patterns in different types of**
245 **tissue**
246 To observe the PpPINA-GFP localization in *P. patens*, we used a stable moss
247 transgenic line carrying the native promoter controlled *PpPINA* genomic DNA-GFP
248 fusion (*pPINA::PpPINA-GFP*) where GFP was inserted in the same position as we
249 verified. The moss *P. patens* has a filamentous protonema stage and a leafy
250 gametophore stage in its life cycle. The initial protonema cell was newly regenerated
251 from a detached leaf, and the elongated protonema was imaged from a 6-days-old
252 moss colony. PpPINA-GFP localized at the PM of the protonema tip with a clear
253 polarity in both initial and elongated protonemata (Figure 4A). To examine whether the
254 polar localization of PpPINA-GFP appears in complex tissues composed of multiple
255 cell layers as well, we observed its localization in gametophytic leaves. In young
256 gametophytic leaves, PpPINA-GFP showed clear basal-apical polarization along the
257 leaf axis with notable corner enrichment (Figure 4A), whereas in mature leaves
258 PpPINA-GFP was evenly distributed on the PM (Supplemental Figure 3). We also
259 analyzed another endogenous *P. patens* PpPINB, fused with GFP and driven by its
260 endogenous promoter. Notably, PpPINB-GFP did not show visible polarity at the tip of
261 protonema, but more even PM distribution with an increased intracellular signal
262 (Supplemental Figure 4). The difference between the localization of PpPINA-GFP and
263 PpPINB-GFP suggests different trafficking and polarization pathways for different PINs
264 co-existing in the same cell already in bryophytes.
265 The divergence of PpPINA-GFP polarity in filamentous protonema cells and in
266 gametophytic leaves made us wondering if this tissue-specific polarization of PINs is
267 conserved in other bryophytes. To achieve this, we looked at another bryophyte, the

268 liverwort *M. polymorpha* that produces gemmae as the asexual reproductive progenies
269 consisted of multiple cell layers. After water imbibition, single-cellular rhizoids emerge
270 from the large rhizoid precursor cells on epidermis of a gemma (Shimamura, 2016).
271 To analyze the subcellular localization of the sole canonical PIN, MpPINZ, in *M.*
272 *polymorpha*, we generated a *p35S::MpPINZ-GFP* transgenic line. Interestingly,
273 MpPINZ-GFP localized on the PM with small intracellular puncta and with no apparent
274 polarity in all gemma epidermal cells (Figure 4B, right panel). However, when gemmae
275 were stimulated to grow rhizoids, the signal of MpPINZ-GFP accumulated at the
276 protrusion site of emerging rhizoids in the rhizoid precursor cells (Figure 4B, yellow
277 arrowheads). Later after their emergence, MpPINZ-GFP was polarized at the tip of
278 young rhizoids (Figure 4B), whereas the signal diminished when the rhizoids
279 elongated.
280 The localization of PpPINA- and MpPINZ-GFP in filamentous and complex
281 tissues suggests distinct polarity recognition mechanisms for bryophytic PINs in
282 different tissue types. To examine if Arabidopsis PINs show similar polar patterns as
283 bryophytic PINs in different types of tissues, we observed *pPIN2::AtPIN2-GFP* line in
284 filamentous root hairs and complex epidermal cells. As previously described, AtPIN2-
285 GFP showed apical localization in epidermal cells (Figure 4C) (Zhang et al., 2019).
286 Since the polarity of bryophytic PINs in their original species mainly appeared at the
287 tip of filamentous tissues, we focused on the localization of AtPIN2-GFP in initial and
288 elongated root hairs, respectively. AtPIN2-GFP revealed a polar localization at the tip
289 of initial root hairs (Figure 4C). However, the polarity of AtPIN2-GFP signals diminished
290 in the elongated hairs (Figure 4C). The different polarity patterns of PINs in different
291 types of tissue support the notion that regulations of PIN polarization are specialized
292 in different cellular profiles and in different developmental contexts.
293
294 **Xenologous PINs are PM localized with no defined polarity**
295 Since bryophytic and Arabidopsis PINs demonstrated tissue- and development-
296 specific polarity regulations, we wonder if the conserved phosphorylation sites in the
297 HL are sufficient to drive the polarization of xenologous PINs in other species. To
298 achieve this, we observed the same moss *XVE::PIN-GFPs* transgenic lines we
299 generated for the auxin export assay, carrying PpPINA-, AtPIN1-, and AtPIN2-GFP,
300 respectively. In protonemata, AtPIN1-GFP showed an even distribution on the PM and
301 cell division plane without apparent polarity at the tips, and displayed numerous small

302 intracellular puncta, whereas the PpPINA-GFP signal presented the same polarization
303 as driven by its endogenous promoter (Figure 4A, 5A, and 5D). AtPIN2-GFP under the
304 same induction condition showed much lower intensity but resembled AtPIN1-GFP
305 localization patterns, we thus took AtPIN1-GFP as representative images
306 (Supplemental Figure 5). A short-term induction of *XVE::AtPIN1-GFP* was performed,
307 and it showed no difference in the localization, which verified that the localization
308 patterns of AtPIN1-GFP were not caused by overexpression (Supplemental Video 1).
309 To investigate whether these features are conserved in bryophytes, we
310 introduced AtPIN1-GFP driven by the *35S* promoter into *M. polymorpha*. In gemma
311 epidermal cells, the AtPIN1-GFP showed a non-polar PM localization with high
312 cytosolic signals (Supplemental Figure 6A). In emerging rhizoids, AtPIN1-GFP did not
313 show visible polar localization in rhizoid precursor cells (Supplemental Figure 6B). In
314 young rhizoids, where MpPINZ-GFP showed clear tip polarization, AtPIN1-GFP was
315 evenly distributed on the PM with homogenized cytosolic signals (Figure 5B and 5D).
316 Since our results indicated that Arabidopsis AtPIN1-GFP in examined
317 bryophytes are delivered to the PM with no visible polarity, we next addressed whether
318 Arabidopsis trafficking machinery can polarize bryophytic PINs. To analyze bryophytic
319 PINs, we observed the protein localization at epidermal cells of transgenic Arabidopsis
320 lines expressing *pPIN2::AtPIN2-, PpPINA-, and MpPINZ-GFP* (Zhang et al., 2019). As
321 previously described, AtPIN2-GFP showed apical localization in the epidermal cells,
322 while PpPINA-GFP localized at both the apical and basal sides and MpPINZ-GFP
323 mainly localized at the basal side with some lateral residence. (Figure 5C and 5E)
324 (Zhang et al., 2019). These data thus support that the machinery driving PIN proteins
325 to the PM through a generally conserved cellular trafficking pathway, whereas the PIN
326 polarization is specialized in different species.
327
328 **Cytoskeletal networks are important for the polarization of bryophytic PINs**
329 The diversification of PIN polarities in different plant species and tissues suggests that
330 plant cells might utilize various machineries to deliver and maintain PIN proteins to the
331 target side on the PM. To verify this, we examined the necessity of the cytoskeletal
332 networks in the polarization of bryophytic PINs and AtPIN2 in their original species.
333 We depolymerized actin filaments or microtubules by treating plant tissues with
334 Latrunculin B (LatB) or Oryzalin (Ory), respectively. In *P. patens*, the abolishment of
335 actin filaments resulted in the hyper-polarization of PpPINA-GFP, where PpPINA-GFP

336 accumulated at a focal locus to the very tip of the cell (Figure 6A and 6C). The
337 disruption of microtubules resulted in less accumulation of PpPINA-GFP at the tip of
338 protonemata, and the PpPINA-GFP appeared to be detached from the PM (Figure 6A
339 and 6C). The changes of PpPINA-GFP localization in response to drug treatments
340 demonstrated the requirement of cytoskeletal networks for PpPINA-GFP polarization
341 in filamentous tissues.

342 In *M. polymorpha*, we used the same pharmacological interference to
343 investigate whether the MpPINZ-GFP polarization in young rhizoids relies on the
344 cytoskeletal networks. MpPINZ-GFP remains polarized at the tip when actin filaments
345 were disrupted, while the disruption of microtubules resulted in the dislocation of the
346 polarized MpPINZ-GFP (Figure 6B and 6C). These results collectively demonstrate
347 the diversification on cytoskeletal dependency for PINs polarization within the
348 bryophyte clade.

349 In Arabidopsis, the disruption of actin filaments by LatB resulted in an increasing
350 appearance of AtPIN2-GFP signals in the cell interior, while the Ory treatment caused
351 a minor effect on AtPIN2-GFP localization (Figure 6D). Upon cytoskeleton disruption,
352 the apical polarization of AtPIN2-GFP in epidermal cells was still evident; suggesting
353 that in contrast to the dependency of cytoskeletal networks for the bryophytic PINs,
354 the polarization of Arabidopsis PINs mainly relies on other trafficking or polarity
355 retention mechanisms. Again, these results reinforce the notion that mechanisms
356 underlying PIN polarization have been expanded and specifically diversified in
357 different species.
358
359
360 **Discussion**
361
362 **Evolution of sequence-specific determinants of PIN polarity**
363 In flowering plants, as exemplified by Arabidopsis, the five PM-localized canonical
364 PINs show different polarities in different developmental and tissue contexts, thus
365 mediating directional auxin fluxes and generating asymmetric auxin distribution for
366 plethora of developmental processes ultimately shaping the plant form. Originating
367 from a single PIN auxin transporter, such as found in simple filamentous streptophyte
368 algae (Skokan et al., 2019), PIN family radiated during evolution into PINs showing
369 different expression and localization patterns and mediating many developmental and

370 physiological functions.

371 Ectopic co-expression of PINs in the same cell type such as AtPIN1 and AtPIN2
372 in root epidermis can lead to diverse polarity patterns (AtPIN1 – basal; AtPIN2 – apical),
373 thus demonstrating simultaneous presence of multiple polarity mechanisms in those
374 cells (Wisniewska et al., 2006). In this study, we showed that in bryophytes, as
375 exemplified by the moss *P. patens*, PpPINA and PpPINB endogenously expressed in
376 protonemata filaments, present different localization patterns (Figure 4 and
377 Supplemental Figure 4). PpPINA shows tip-focused PM localization, whereas PpPINB
378 can be found more spread on the PM and also intracellularly. Whereas, the functional
379 importance of this difference remains unclear, it clearly shows that already in
380 bryophytes, parallel polarity/trafficking mechanisms exists in the same cells, to which
381 different PINs can be recruited, presumably based on specific sequence-based signals.

382 Notably, the sequence alignment between the HL regions of PpPINA and
383 PpPINB showed 90.31% identity, suggesting that these signals are presumably
384 encoded within the 10% difference regions. Further analysis of the differences
385 between PpPINA and PpPINB or AtPIN1 and AtPIN2 would help to identify the
386 sequence signals for PIN polarity regulations. Despite the identity of the sequence-
387 based signals remain unclear, our observations show that cellular polarity mechanisms
388 and PIN sequence-based polarity signals, which are crucial for diverse developmental
389 roles in flowering plants, started to diversify already in bryophytes.

390

391 **Context-specific determinants of PIN polarity**

392 It is well known from Arabidopsis that the same PINs show different localization
393 patterns in different contexts (Vieten et al., 2005). For example, AtPIN2 is apicalized
394 in epidermal cells, while it is localized on the basal side of young cortex cells (Kleine-
395 Vehn *et al.*, 2008a). The observations imply that different cell types possess specific
396 trafficking pathways for the same PIN protein. In line with this, our results show that in
397 filamentous cells, e.g., protonemata in *P. patens*, rhizoids in *M. polymorpha*, and root
398 hairs in Arabidopsis, endogenous PIN proteins are polarized at the tip of apical cells
399 (Figure 4A-4C). Notably, MpPINZ-GFP and AtPIN2-GFP signals were diminished
400 when the rhizoids or root hairs elongated, and the PpPINA-GFP was polarized only in
401 young gametophytic leaves but the pattern dispersed in mature leaves. These data
402 collectively demonstrate that PIN polarity is differentially regulated in different
403 developmental contexts.

404 In complex tissues with multiple cell layers, unlike in filamentous tissues, the
405 PM-localized MpPINZ-GFP did not show polarity in thalli, while PpPINA-GFP and
406 AtPIN2-GFP presented polar localization at the apical-basal domain of the cells
407 (Figure 4A-4C). This data shows that PIN polarity and trafficking mechanisms have
408 evolved with specific modifications in different tissues and cell types, in both
409 angiosperms and early-diverging land plants. This likely reflects different requirements
410 for directional auxin transport in different developmental contexts, and it implies a co-
411 evolution of PIN sequence-based signals and cell type-specific polar sorting and
412 trafficking mechanisms.
413
414 **Diversification of PIN trafficking and polarity mechanisms during land plant**
415 **evolution**
416 The core mechanisms for auxin biosynthesis, auxin signaling, and PIN-mediated auxin
417 transport are evolutionary conserved across land plants (Blazquez et al., 2020; Kato
418 et al., 2018; Sauer and Kleine-Vehn, 2019). However, bryophytes and vascular plants
419 diverged around 450 million years ago and emerged different types of tissues and
420 organs, it is not clear how conserved the PIN polarity regulation is under such drastic
421 changes during land plant evolution. Our cross-species studies revealed that
422 xenologous PINs, such as Arabidopsis PINs in bryophytes and bryophytic PINs in
423 Arabidopsis, are able to traffic to the PM (Figure 5), which suggests that all canonical
424 PINs can be recognized by the general protein transport machinery in other species.
425 Interestingly, when the Arabidopsis PINs are ectopically expressed in
426 bryophytes, they fail to form any specific polarity, whereas bryophytic PINs remain in
427 apical-basal domains in Arabidopsis epidermis (Figure 5). These observations may
428 hint an evolutionary loss of some regulatory motifs for PIN polarization that are
429 presence in bryophytic PINs but absence in Arabidopsis PINs. In line with this, the
430 overall coding sequences of bryophytic PINs are longer than Arabidopsis PINs, and
431 the extra sequences are positioned in their HLs, the main regulatory regions for PIN
432 polarization. Our study thus demonstrates that PINs polarity mechanisms are not
433 conserved throughout plant evolution.
434 This notion was also verified by the differences in cytoskeleton requirements
435 for PIN polarization between bryophytes and angiosperms. The polarity of bryophytic
436 PINs was disrupted when cytoskeletal networks are depolymerized, while Arabidopsis
437 AtPIN2 was not affected (Figure 6). This finding suggests a gradual shift in the

438 dependence of PIN polarity and trafficking from the cytoskeleton-dependent pathways
439 towards the cytoskeleton-independent pathways along the land plant evolution.
440 Overall, our results demonstrate that different plant species evolved specialized
441 pathways to deliver PINs and maintain their polarity at the PM. This is likely linked to
442 an increasing repertoire of auxin transport developmental roles adopted with
443 increasing morphological complexity during land plant evolution.
444
445 **Methods**
446
447 **Plant growth and transformation**
448 Arabidopsis seeds were surface sterilized and grown on 1/2 MS plates. After a two-
449 day stratification at 4°C, seedlings were grown under the long-day condition (16 hours
450 light, 8 hours dark) at 22°C with 100-120 μmol photons $m^{-2}s^{-1}$ white light. For *P. patens*,
451 all transgenic and WT plants were cultured on BCD medium plates in a growth
452 chamber at 24°C under the long-day condition (16 hours light, 8 hours dark) with
453 35μmol photons $m^{-2}s^{-1}$ white light. For *M. polymorpha*, WT and all transgenic plants
454 were cultured on 1/2 B5 plates in a growth chamber under the long-day condition (16
455 hours light, 8 hours dark) at 22°C with 50-60 μmol photons $m^{-2}s^{-1}$ white LED light.
456 All transgenic plants used in this study are listed in Supplemental Table 1. *P.*
457 *patens* transgenic plants *pPINA::PINA-GFP* has been generated and verified as
458 previously reported (Viaene et al., 2014), and the inducible overexpression
459 XVE::AtPIN1-GFP, *XVE::AtPIN2-GFP*, and *XVE::MpPINZ-GFP* lines were generated
460 as described in previous studies (Tang et al., 2020; Yamada et al., 2016). In brief, the
461 Gransden 2004 WT moss plants were freshly propagated and transformed via the
462 PEG-mediated transformation (Nishiyama et al., 2000). The transformants were
463 selected under Hygromycin (20μg/mL), and two independent transgenic lines were
464 selected for imaging and analysis.
465 *p35S::MpPINZ-, AtPIN1-,* and *AtPIN2-GFP M. polymorpha* plants were
466 generated via the Agrobacterium transformation method described before (Kubota et
467 al., 2013). In brief, the apical meristemic region of each two-week-old Takaragaike-1
468 (Tak-1) thallus was removed and further cut into four pieces. After culturing on 1/2 B5
469 with 1% sucrose agar plates for 3 days, the cut thalli were transferred to 50ml 0M51C
470 medium with 200 μM acetosyringone (4'-Hydroxy-3',5'-dimethoxyacetophenone) in

471 200ml flasks with 130 rpm agitation to coculture with OD_{600} = 1 density agrobacteria
472 harboring the target construct for another 3 days. The transformed thalli were washed
473 and plated on 1/2 B5 plates with proper antibiotic selection. Independent T1 lines were
474 isolated, and G1 lines from independent T1 lines were generated by sub-cultivating
475 single gemmalings, which emerged asexually from a single initial cell (Shimamura,
476 2016). The next generation of G1, called the G2 generation, was used for analyses.
477 Arabidopsis transgenic lines bearing bryophytic PIN-GFPs under *AtPIN2* promoter
478 control were generated and used as in a previous study (Zhang et al., 2019). For root
479 imaging, seeds were sown on 1/2 Murashige–Skoog (MS) medium plates and kept at
480 4°C for 2 days and moved to the growth chamber to culture vertically for another 4
481 days.
482
483 **Plasmid construction**
484 Plasmids and primers for construction and genotype confirmation are listed in
485 Supplemental Table 2. For transgenic lines with inducible overexpression by moss, the
486 insertion site of the *GFP* gene into the HL was indicated in Figure 3A, and the *PIN-*
487 *GFP* regions were amplified from previously generated plasmids (Zhang et al., 2019)
488 by PCR and cloned into the gateway entry plasmid pENTR/D-TOPO® as the
489 manufacturer suggested. The fragments were sub-cloned into the pPGX8 vector,
490 which contains a p*35S* driven β-estradiol inducible XVE cassette (Floriach-Clark et al.,
491 2021; Kubo et al., 2013; Nakaoka et al., 2012) via a Gateway® LR reaction (Invitrogen)
492 as the manufacture's recommendation.
493 To generate a *p35S::MpPINZ-, AtPIN1-*, and *AtPIN2-GFP* construct, the cDNA
494 of the target fragment containing proper *GFP* insertion were amplified with the primers
495 listed in Supplemental Table 2. The amplified fragments were cloned into the
496 pENTR/D-TOPO® vector (Invitrogen) with the protocol supplied by the manufacturer.
497 Plasmids with target genes were further sub-cloned into the pMpGWB102 vector
498 containing a *35S* promoter (Ishizaki et al., 2015) by the Gateway® LR reaction
499 (Invitrogen) as the manufacturer's recommendation.
500
501 **Microscopy**
502 For moss observation, protonemata were cultured in glass-bottom dishes covered by
503 BCD agar medium for 6 – 7d. The live-cell imaging was then performed on a Leica
504 SP8X-SMD confocal microscope equipped with a hybrid single-molecule detector

505 (HyD) and an ultrashort pulsed white-light laser (WLL; 50%; 1 ps at 40 MHz frequency).
506 The Leica Application Suite X was used as a software platform, and imaging was
507 conducted with a HC PL APO CS2 40x/1.20 water immersion objective. The following
508 settings were used: scan speed of 400 Hz, resolution of 1024 x 1024 pixels and
509 standard acquisition mode of the hybrid detector. The time-gating system was
510 activated to avoid the autofluorescence emitted from chloroplasts. For the filament
511 growth assay, the imaging dish was applied with FM4-64 (Invitrogen) solution for 10-
512 30 mins, and the 10x objective lens was used.
513 For Marchantia observation, gemmae were picked from a gemma cup and
514 transferred into a 24-well plate with 500 μl liquid 1/2 B5 medium. After culturing in the
515 growth chamber for 24 hours, gemmae from each sample were transferred and
516 observed on a slide under Leica Stellaris 8 system with HyD detectors and the
517 ultrashort pulsed white-light laser (WLL; 70%; 1 ps at 40 MHz frequency). The Leica
518 Application Suite X was used as a software platform, and imaging was conducted with
519 an HC PL APO CS2 40x/1.20 water immersion objective. The following settings were
520 used: scan speed of 400 Hz and resolution of 1024 x 1024 pixels. For GFP-containing
521 images, a 488nm white light laser was selected, and the detection range was set
522 between 500nm to 525nm. The tau-gating model, harvesting photons with 1.0-10.0ns
523 lifetime, was used for all Marchantia imaging to avoid autofluorescence emitted from
524 the chloroplasts. For the surface section (rhizoid precursor cell observation), a 5 μm-
525 thick section was set using the z-section method with auto-optimization spacing to
526 capture rhizoids' protrusion.
527 For Arabidopsis root imaging, 4-day-old seedlings of each indicated genotype
528 were used for fluorescence imaging. After treatment in the liquid MS medium supplied
529 with indicated chemicals, seedlings were carefully mounted on a slice with growth
530 medium and then placed into a chambered coverslip (Lab-Tek) for imaging. For the
531 root hair imaging, a 3 μm Z-projection image with 1 μm step was taken around the
532 medium plan of the root hair. All fluorescence imaging was performed using a laser
533 scanning confocal microscopy (Zeiss LSM800, 20x air lens). The default setting for
534 GFP detection was applied with 488nm excitation and 495-545nm emission.
535
536 **Images quantification**
537 All images were analyzed by Fiji (ImageJ, https://imagej.net/software/fiji/). For the

538 polarization patterns at the tip of filaments in *P. patens*, a line with 5 px thickness was
539 plotted along the PM as depicted in Figure 4 and Figure 5. The representative images
540 for the DMSO control and drug treatments, obtained from the same imaging settings,
541 were used to draw the line, and the mean intensity along the line was shown. For the
542 moss phenotype analysis, mosses bearing inducible *PIN-GFP* were cultivated in the
543 imaging dish for 5 days, followed by 1 μM β-estradiol induction for another 3 days. The
544 cell outlines were stained with FM4-64 for 10-30 mins. The line drawing function in Fiji
545 was used to measure the length of subapical cell, and the line was depicted between
546 the middle points of the two cell division planes. The angle measurement function was
547 applied to examine the angle between the first cell division plane and horizontal cell
548 outline for the division angle measurement.
549
550 **Genomic DNA isolation**
551 The genomic DNA of transformants was isolated by the cetyltrimethylammonium
552 bromide (CTAB) gDNA extraction (Schlink and Reski, 2002). In brief, moss tissues
553 were harvested from one full plate and were ground in liquid nitrogen. The ground
554 tissues were then mixed and were incubated with a CTAB buffer, followed by the
555 addition of chloroform. After centrifugation, the supernatant was collected and was
556 precipitated with isopropanol at -20°C for one hour.
557
558 **Pharmacological treatments**
559 To depolymerize microtubules and actin filaments, we used oryzalin (Sigma) and
560 latrunculin B (Sigma) to treat plants. The concentration and duration of treatment for
561 different plants have been given in numbers, and the conditions we used have been
562 shown to efficiently depolymerize cytoskeletal networks in different species (Baluska
563 et al., 2001; Baskin et al., 1994; Glanc et al., 2019; Oda et al., 2009; Vidali et al., 2009).
564 For *P. patens*, the chemical was diluted in a liquid BCD medium and was applied to
565 the imaging dishes before imaging.
566 For *M. polymorpha*, G2 gemmae from transgenic plants were transferred into
567 each well of a 24-well plate containing 500 μl liquid 1/2 B5 medium and cultured in the
568 growth chamber for 16 hours. The chemicals were diluted directly into the medium
569 prior to imaging at the time indicated in the text. Based on previous studies, the
570 concentration of Ory (Era et al., 2013) and LatB (Otani et al., 2018) were selected.
571 For Arabidopsis, 4-days-old seedlings were submerged into the liquid MS medium

572 supplied with chemicals and then transferred to another agar medium for imaging.
573 0.1% DMSO (Duchefa; 10 mM dimethylsulfoxide) was used as control for all
574 treatments.
575
576 ***P. patens* auxin export assay**
577 The auxin export assay performed with transgenic moss plants was modified based
578 on the protocol developed for Arabidopsis seedlings (Lewis and Muday, 2009). In brief,
579 7-days-old fresh tissues were transfer to liquid BCDAT growth medium with 1μM β-
580 estradiol induction for another 4d with gentle shaking, followed by ^{3}H-IAA treatment
581 with a final concentration of 10 nM for 24 hrs. The radioactive tissues were then
582 washed twice with sterile H_2O, and were cultivated in fresh BCDAT medium for another
583 24 hrs. The cultivated medium was then collected to mix with ScintiVerse BD cocktail
584 (Fisher, SX18-4) in 1:30 (v:v), and the export of auxin was measured by the
585 Scintillation counter (Beckman, LS6500).
586
587 ***M. polymorpha* thallus growth assay**
588 G2 gemmae were transferred onto 1/2 B5 agar plates and grew for 10 days. Gemmae
589 were imaged under a dissecting microscope (SZN71, LiWeng, Taiwan) with a CCD
590 camera (Polychrome M, LiWeng, Taiwan). For measuring the vertical growth angle, an
591 agar cube with an individual plant was cut out from the plate and placed in the middle
592 of a slide. The slide was put on the surface of a laminar flow at a fixed distance to the
593 edge, and images were taken by an HTC U11 cell phone camera. The growth angle
594 was further measured by using ImageJ (https://imagej.net/software/fiji/).
595
596 **Phylogenetic analysis**
597 The phylogenetic analysis for full length amino acid sequences of all examined PINs
598 was carried out in MEGA X program (Kumar et al., 2018) and the results were imported
599 into iTOL (https://itol.embl.de/) for visual illustration. The evolutionary history was
600 inferred by using the Maximum Likelihood method and JTT matrix-based model with
601 default settings (Jones et al., 1992). The alignment and identity index were produced
602 by online CLUSTAL alignment program with default settings.
603
604 **Funding**
605 This work was supported by the ERC grant (PR1023ERC02) to H. T. and J. F., and by

the ministry of science and technology (grant number 110-2636-B-005-001) to K. J. L.

Author contributions

H. T., K. J. L., and J. F. designed experiments. Y.Z. C. initiated the project and provided key constructs and materials. H. T. performed and analyzed all the *P. patens* and Arabidopsis related experiments with the help of Y. L. C. and S. L. T.. K. J. L. performed and analyzed all the *M. polymorpha* related experiments. H. T., K. J. L, and J. F. wrote the manuscript.

Acknowledgments

The authors would like to thank Dr. A. Johnson and Ms. Alexandra Mally for their careful proofreading. We also thank Dr. T. Kohchi for sharing the pMpGWB102 vector (Addgene #68556; http://n2t.net/addgene:68556; RRID:Addgene_68556).

References

Abas, L., Benjamins, R., Malenica, N., Paciorek, T., Wisniewska, J., Moulinier-Anzola, J.C., Sieberer, T., Friml, J., and Luschnig, C. (2006). Intracellular trafficking and proteolysis of the Arabidopsis auxin-efflux facilitator PIN2 are involved in root gravitropism. Nat Cell Biol **8**:249-256. 10.1038/ncb1369.

Adamowski, M., and Friml, J. (2015). PIN-dependent auxin transport: action, regulation, and evolution. Plant Cell **27**:20-32. 10.1105/tpc.114.134874.

Baluska, F., Jasik, J., Edelmann, H.G., Salajova, T., and Volkmann, D. (2001). Latrunculin B-induced plant dwarfism: Plant cell elongation is F-actin-dependent. Dev Biol **231**:113-124. 10.1006/dbio.2000.0115.

Barbosa, I.C.R., Hammes, U.Z., and Schwechheimer, C. (2018). Activation and Polarity Control of PIN-FORMED Auxin Transporters by Phosphorylation. Trends Plant Sci **23**:523-538. 10.1016/j.tplants.2018.03.009.

Baskin, T.I., Wilson, J.E., Cork, A., and Williamson, R.E. (1994). Morphology and microtubule organization in Arabidopsis roots exposed to oryzalin or taxol. Plant Cell Physiol **35**:935-942.

Bennett, T.A., Liu, M.M., Aoyama, T., Bierfreund, N.M., Braun, M., Coudert, Y., Dennis, R.J., O'Connor, D., Wang, X.Y., White, C.D., et al. (2014). Plasma membrane-targeted PIN proteins drive shoot development in a moss. Curr Biol **24**:2776-2785. 10.1016/j.cub.2014.09.054.

Blazquez, M.A., Nelson, D.C., and Weijers, D. (2020). Evolution of Plant Hormone Response Pathways. Annu Rev Plant Biol **71**:327-353. 10.1146/annurev-arplant-050718-100309.

Doyle, S.M., Haeger, A., Vain, T., Rigal, A., Viotti, C., Langowska, M., Ma, Q., Friml, J., Raikhel, N.V., Hicks, G.R., et al. (2015). An early secretory pathway mediated by GNOM-LIKE 1 and GNOM is essential for basal polarity establishment in Arabidopsis thaliana. Proc Natl Acad Sci U S A **112**:E806-815. 10.1073/pnas.1424856112.

643 **Era, A., Kutsuna, N., Higaki, T., Hasezawa, S., Nakano, A., and Ueda, T.** (2013). Microtubule
644 stability affects the unique motility of F-actin in Marchantia polymorpha. J Plant Res
645 **126**:113-119. 10.1007/s10265-012-0496-4.
646 **Floriach-Clark, J., Tang, H., and Willemsen, V.** (2021). Mosses: Accessible Systems for Plant
647 Development Studies. In Model Organisms in Plant Genetics, (IntechOpen.
648 **Friml, J.** (2021). Fourteen Stations of Auxin. Cold Spring Harb Perspect Biol **14**:a039859.
649 10.1101/cshperspect.a039859.
650 **Friml, J., Yang, X., Michniewicz, M., Weijers, D., Quint, A., Tietz, O., Benjamins, R.,**
651 **Ouwerkerk, P.B., Ljung, K., Sandberg, G., et al.** (2004). A PINOID-dependent binary switch in
652 apical-basal PIN polar targeting directs auxin efflux. Science **306**:862-865.
653 10.1126/science.1100618.
654 **Geldner, N., Friml, J., Stierhof, Y.D., Jurgens, G., and Palme, K.** (2001). Auxin transport
655 inhibitors block PIN1 cycling and vesicle trafficking. Nature **413**:425-428. 10.1038/35096571.
656 **Glanc, M., Fendrych, M., and Friml, J.** (2018). Mechanistic framework for cell-intrinsic re-
657 establishment of PIN2 polarity after cell division. Nat Plants **4**:1082-1088. 10.1038/s41477-
658 018-0318-3.
659 **Glanc, M., Fendrych, M., and Friml, J.** (2019). PIN2 Polarity Establishment in Arabidopsis in
660 the Absence of an Intact Cytoskeleton. Biomolecules **9**:222. 10.3390/biom9060222.
661 **Ishizaki, K., Nishihama, R., Ueda, M., Inoue, K., Ishida, S., Nishimura, Y., Shikanai, T., and**
662 **Kohchi, T.** (2015). Development of Gateway Binary Vector Series with Four Different
663 Selection Markers for the Liverwort Marchantia polymorpha. PLoS One **10**:e0138876.
664 10.1371/journal.pone.0138876.
665 **Jones, D.T., Taylor, W.R., and Thornton, J.M.** (1992). The rapid generation of mutation data
666 matrices from protein sequences. Comput Appl Biosci **8**:275-282.
667 10.1093/bioinformatics/8.3.275.
668 **Jumper, J., Evans, R., Pritzel, A., Green, T., Figurnov, M., Ronneberger, O.,**
669 **Tunyasuvunakool, K., Bates, R., Zidek, A., Potapenko, A., et al.** (2021). Highly accurate
670 protein structure prediction with AlphaFold. Nature **596**:583-589. 10.1038/s41586-021-
671 03819-2.
672 **Kato, H., Nishihama, R., Weijers, D., and Kohchi, T.** (2018). Evolution of nuclear auxin
673 signaling: lessons from genetic studies with basal land plants. J Exp Bot **69**:291-301.
674 10.1093/jxb/erx267.
675 **Kato, H., Kouno, M., Takeda, M., Suzuki, H., Ishizaki, K., Nishihama, R., and Kohchi, T.**
676 (2017). The Roles of the Sole Activator-Type Auxin Response Factor in Pattern Formation of
677 Marchantia polymorpha. Plant Cell Physiol **58**:1642-1651. 10.1093/pcp/pcx095.
678 **Kleine-Vehn, J., Langowski, L., Wisniewska, J., Dhonukshe, P., Brewer, P.B., and Friml, J.**
679 (2008a). Cellular and molecular requirements for polar PIN targeting and transcytosis in
680 plants. Mol Plant **1**:1056-1066. 10.1093/mp/ssn062.
681 **Kleine-Vehn, J., Dhonukshe, P., Sauer, M., Brewer, P.B., Wisniewska, J., Paciorek, T.,**
682 **Benkova, E., and Friml, J.** (2008b). ARF GEF-dependent transcytosis and polar delivery of PIN
683 auxin carriers in Arabidopsis. Curr Biol **18**:526-531. 10.1016/j.cub.2008.03.021.
684 **Kleine-Vehn, J., Wabnik, K., Martiniere, A., Langowski, L., Willig, K., Naramoto, S., Leitner,**
685 **J., Tanaka, H., Jakobs, S., Robert, S., et al.** (2011). Recycling, clustering, and endocytosis
686 jointly maintain PIN auxin carrier polarity at the plasma membrane. Mol Syst Biol **7**:540.
687 10.1038/msb.2011.72.
688 **Krecek, P., Skupa, P., Libus, J., Naramoto, S., Tejos, R., Friml, J., and Zazimalova, E.** (2009).
689 The PIN-FORMED (PIN) protein family of auxin transporters. Genome Biol **10**:249.

690 10.1186/gb-2009-10-12-249.
691 **Kubo, M., Imai, A., Nishiyama, T., Ishikawa, M., Sato, Y., Kurata, T., Hiwatashi, Y., Reski, R.,**
692 **and Hasebe, M.** (2013). System for stable beta-estradiol-inducible gene expression in the
693 moss Physcomitrella patens. PLoS One **8**:e77356. 10.1371/journal.pone.0077356.
694 **Kubota, A., Ishizaki, K., Hosaka, M., and Kohchi, T.** (2013). Efficient Agrobacterium-
695 mediated transformation of the liverwort Marchantia polymorpha using regenerating thalli.
696 Biosci Biotechnol Biochem **77**:167-172. 10.1271/bbb.120700.
697 **Kumar, S., Stecher, G., Li, M., Knyaz, C., and Tamura, K.** (2018). MEGA X: Molecular
698 Evolutionary Genetics Analysis across Computing Platforms. Mol Biol Evol **35**:1547-1549.
699 10.1093/molbev/msy096.
700 **Lavy, M., Prigge, M.J., Tao, S., Shain, S., Kuo, A., Kirchsteiger, K., and Estelle, M.** (2016).
701 Constitutive auxin response in Physcomitrella reveals complex interactions between Aux/IAA
702 and ARF proteins. Elife **5**:e13325. 10.7554/eLife.13325.
703 **Lewis, D.R., and Muday, G.K.** (2009). Measurement of auxin transport in Arabidopsis
704 thaliana. Nat Protoc **4**:437-451. 10.1038/nprot.2009.1.
705 **Leyser, O.** (2018). Auxin Signaling. Plant Physiol **176**:465-479. 10.1104/pp.17.00765.
706 **Michniewicz, M., Zago, M.K., Abas, L., Weijers, D., Schweighofer, A., Meskiene, I., Heisler,**
707 **M.G., Ohno, C., Zhang, J., Huang, F., et al.** (2007). Antagonistic regulation of PIN
708 phosphorylation by PP2A and PINOID directs auxin flux. Cell **130**:1044-1056.
709 10.1016/j.cell.2007.07.033.
710 **Mockaitis, K., and Estelle, M.** (2008). Auxin receptors and plant development: a new
711 signaling paradigm. Annu Rev Cell Dev Biol **24**:55-80.
712 10.1146/annurev.cellbio.23.090506.123214.
713 **Nakaoka, Y., Miki, T., Fujioka, R., Uehara, R., Tomioka, A., Obuse, C., Kubo, M., Hiwatashi,**
714 **Y., and Goshima, G.** (2012). An inducible RNA interference system in Physcomitrella patens
715 reveals a dominant role of augmin in phragmoplast microtubule generation. Plant Cell
716 **24**:1478-1493. 10.1105/tpc.112.098509.
717 **Narasimhan, M., Johnson, A., Prizak, R., Kaufmann, W.A., Tan, S., Casillas-Perez, B., and**
718 **Friml, J.** (2020). Evolutionarily unique mechanistic framework of clathrin-mediated
719 endocytosis in plants. Elife **9**10.7554/eLife.52067.
720 **Narasimhan, M., Gallei, M., Tan, S., Johnson, A., Verstraeten, I., Li, L., Rodriguez, L., Han,**
721 **H., Himschoot, E., Wang, R., et al.** (2021). Systematic analysis of specific and nonspecific
722 auxin effects on endocytosis and trafficking. Plant Physiol **186**:1122-1142.
723 10.1093/plphys/kiab134.
724 **Nishiyama, T., Hiwatashi, Y., Sakakibara, I., Kato, M., and Hasebe, M.** (2000). Tagged
725 mutagenesis and gene-trap in the moss, Physcomitrella patens by shuttle mutagenesis. DNA
726 Res **7**:9-17. 10.1093/dnares/7.1.9.
727 **Oda, Y., Hirata, A., Sano, T., Fujita, T., Hiwatashi, Y., Sato, Y., Kadota, A., Hasebe, M., and**
728 **Hasezawa, S.** (2009). Microtubules regulate dynamic organization of vacuoles in
729 Physcomitrella patens. Plant Cell Physiol **50**:855-868. 10.1093/pcp/pcp031.
730 **Omelyanchuk, N.A., Kovrizhnykh, V.V., Oshchepkova, E.A., Pasternak, T., Palme, K., and**
731 **Mironova, V.V.** (2016). A detailed expression map of the PIN1 auxin transporter in
732 Arabidopsis thaliana root. BMC Plant Biol **16 Suppl 1**:5. 10.1186/s12870-015-0685-0.
733 **Otani, K., Ishizaki, K., Nishihama, R., Takatani, S., Kohchi, T., Takahashi, T., and Motose, H.**
734 (2018). An evolutionarily conserved NIMA-related kinase directs rhizoid tip growth in the
735 basal land plant Marchantia polymorpha. Development **145**:dev154617.
736 10.1242/dev.154617.

Pettersen, E.F., Goddard, T.D., Huang, C.C., Meng, E.C., Couch, G.S., Croll, T.I., Morris, J.H., and Ferrin, T.E. (2021). UCSF ChimeraX: Structure visualization for researchers, educators, and developers. Protein Sci **30**:70-82. 10.1002/pro.3943.

Rensing, S.A., Goffinet, B., Meyberg, R., Wu, S.Z., and Bezanilla, M. (2020). The Moss Physcomitrium (Physcomitrella) patens: A Model Organism for Non-Seed Plants. Plant Cell **32**:1361-1376. 10.1105/tpc.19.00828.

Sauer, M., and Kleine-Vehn, J. (2019). PIN-FORMED and PIN-LIKES auxin transport facilitators. Development **146**:dev.168088. 10.1242/dev.168088.

Schlink, K., and Reski, R. (2002). Preparing high-quality DNA from moss (Physcomitrella patens). Plant Molecular Biology Reporter **20**:423-423.

Shimamura, M. (2016). Marchantia polymorpha: Taxonomy, Phylogeny and Morphology of a Model System. Plant Cell Physiol **57**:230-256. 10.1093/pcp/pcv192.

Skokan, R., Medvecka, E., Viaene, T., Vosolsobe, S., Zwiewka, M., Muller, K., Skupa, P., Karady, M., Zhang, Y., Janacek, D.P., et al. (2019). PIN-driven auxin transport emerged early in streptophyte evolution. Nat Plants **5**:1114-1119. 10.1038/s41477-019-0542-5.

Smit, M.E., and Weijers, D. (2015). The role of auxin signaling in early embryo pattern formation. Curr Opin Plant Biol **28**:99-105. 10.1016/j.pbi.2015.10.001.

Sukumar, P., Edwards, K.S., Rahman, A., Delong, A., and Muday, G.K. (2009). PINOID kinase regulates root gravitropism through modulation of PIN2-dependent basipetal auxin transport in Arabidopsis. Plant Physiol **150**:722-735. 10.1104/pp.108.131607.

Tang, H., Duijts, K., Bezanilla, M., Scheres, B., Vermeer, J.E.M., and Willemsen, V. (2020). Geometric cues forecast the switch from two- to three-dimensional growth in Physcomitrella patens. New Phytol **225**:1945-1955. 10.1111/nph.16276.

Tao, S., and Estelle, M. (2018). Mutational studies of the Aux/IAA proteins in Physcomitrella reveal novel insights into their function. New Phytol **218**:1534-1542. 10.1111/nph.15039.

Ung, K.L., Winkler, M., Schulz, L., Kolb, M., Janacek, D.P., Dedic, E., Stokes, D.L., Hammes, U.Z., and Pedersen, B.P. (2022). Structures and mechanism of the plant PIN-FORMED auxin transporter. Nature **609**:605-610. 10.1038/s41586-022-04883-y.

Vanneste, S., and Friml, J. (2009). Auxin: a trigger for change in plant development. Cell **136**:1005-1016. 10.1016/j.cell.2009.03.001.

Viaene, T., Delwiche, C.F., Rensing, S.A., and Friml, J. (2013). Origin and evolution of PIN auxin transporters in the green lineage. Trends Plant Sci **18**:5-10. 10.1016/j.tplants.2012.08.009.

Viaene, T., Landberg, K., Thelander, M., Medvecka, E., Pederson, E., Feraru, E., Cooper, E.D., Karimi, M., Delwiche, C.F., Ljung, K., et al. (2014). Directional auxin transport mechanisms in early diverging land plants. Curr Biol **24**:2786-2791. 10.1016/j.cub.2014.09.056.

Vidali, L., Rounds, C.M., Hepler, P.K., and Bezanilla, M. (2009). Lifeact-mEGFP reveals a dynamic apical F-actin network in tip growing plant cells. PLoS One **4**:e5744. 10.1371/journal.pone.0005744.

Vieten, A., Vanneste, S., Wisniewska, J., Benkova, E., Benjamins, R., Beeckman, T., Luschnig, C., and Friml, J. (2005). Functional redundancy of PIN proteins is accompanied by auxin-dependent cross-regulation of PIN expression. Development **132**:4521-4531. 10.1242/dev.02027.

Wisniewska, J., Xu, J., Seifertova, D., Brewer, P.B., Ruzicka, K., Blilou, I., Rouquie, D., Benkova, E., Scheres, B., and Friml, J. (2006). Polar PIN localization directs auxin flow in plants. Science **312**:883. 10.1126/science.1121356.

784 **Yamada, M., Miki, T., and Goshima, G.** (2016). Imaging Mitosis in the Moss Physcomitrella
785 patens. Methods Mol Biol **1413**:263-282. 10.1007/978-1-4939-3542-0_17.
786 **Yang, Z., Xia, J., Hong, J., Zhang, C., Wei, H., Ying, W., Sun, C., Sun, L., Mao, Y., Gao, Y., et al.**
787 (2022). Structural insights into auxin recognition and efflux by Arabidopsis PIN1. Nature
788 **609**:611-615. 10.1038/s41586-022-05143-9.
789 **Yu, Z., Zhang, F., Friml, J., and Ding, Z.** (2022). Auxin signaling: Research advances over the
790 past 30 years. J Integr Plant Biol **64**:371-392. 10.1111/jipb.13225.
791 **Zhang, J., Nodzynski, T., Pencik, A., Rolcik, J., and Friml, J.** (2010). PIN phosphorylation is
792 sufficient to mediate PIN polarity and direct auxin transport. Proc Natl Acad Sci U S A
793 **107**:918-922. 10.1073/pnas.0909460107.
794 **Zhang, Y., Xiao, G., Wang, X., Zhang, X., and Friml, J.** (2019). Evolution of fast root
795 gravitropism in seed plants. Nat Commun **10**:3480. 10.1038/s41467-019-11471-8.
796 **Zourelidou, M., Absmanner, B., Weller, B., Barbosa, I.C., Willige, B.C., Fastner, A., Streit, V.,**
797 **Port, S.A., Colcombet, J., de la Fuente van Bentem, S., et al.** (2014). Auxin efflux by PIN-
798 FORMED proteins is activated by two different protein kinases, D6 PROTEIN KINASE and
799 PINOID. Elife **3**:e02860. 10.7554/eLife.02860.
800 **Zwiewka, M., Bilanovicova, V., Seifu, Y.W., and Nodzynski, T.** (2019). The Nuts and Bolts of
801 PIN Auxin Efflux Carriers. Front Plant Sci **10**:985. 10.3389/fpls.2019.00985.
802

803

804 **Figure legends**

805

806 **Figure 1. Phosphorylation sites are highly conserved between bryophytic and Arabidopsis**
807 **PINs.**

808 (A) Phylogenetic analysis of canonical PINs from early-divergent plants *P. patens (Pp), M.*
809 *polymorpha (Mp),* and representative angiosperm *A. thaliana (At)*. The unrooted tree
810 shows the relationships of different PINs in two representative bryophytes and
811 Arabidopsis. The scale bar represents the number of changes per site.

812 (B) Identity indexes of all PINs compared to AtPIN2 with full length or only the hydrophilic
813 loop region of coding amino acid sequences. Identity indexes of all PINs compared to
814 AtPIN1 is shown in Supplemental Figure 1.

815 (C) Alignment of PIN amino acid sequences. Identical amino acids are highlighted with
816 blue column. The rea and green boxes show the hydrophilic loop regions bearing
817 conserved phosphorylation sites, which are enlarged in (D).

818 (D) Four conserved phosphorylation sites, labeled by S1 to S4, were verified in previous
819 AtPIN2 studies and are depicted with black frames. Note that S1 to S4 are conserved
820 in every examined PINs.

821

822 **Figure 2. The hydrophilic loops in AtPIN2, PpPINA, and MpPINZ are less conserved.**

823 (A) Structural alignment of AtPIN1 and AtPIN2. The protein structures are predicted by
824 Alphafold2 and aligned in ChimeraX software. The structural conserved regions are
825 indicated by black arrowheads, and the non-conserved regions are indicated by empty
826 arrowheads.

827 (B) Structural alignment of AtPIN2 with PpPINA and MpPINZ. Only transmembrane
828 domains and one loop aligned with each other, while the majority of hydrophilic loop
829 regions are not conserved. The four conserved phosphorylation sites are labeled with
830 atom details in ball-and-stick style.

831 (C) – (E) Individual protein structure retrieved from (B). The four conserved
832 phosphorylation sites are indicated by arrowheads.

833

834 **Figure 3. GFP-fused PIN proteins possess auxin export activity.**

835 (A) The insertion site of GFP in indicated PIN proteins. Numbers represent the amino acid
836 position in respective proteins.

837 (B) The auxin export assay with *P. patens* transgenic plants. Fresh tissues were incubated
838 with radioactive H^3 IAA, followed by washing and the radiative H^3-IAA exported in the
839 new culture medium was measured with the scintillation detector after one day.

840 (C) Representative protonema cells of the indicated genetic background. The cell outline
841 was stained with FM4-64. White arrowheads indicate the first cell division plane, and
842 the yellow double arrow indicates the cell length of the subapical cell. Scale bar = 100
843 µm.

844 (D) and (E), Quantitative results of the subapical cell length and the division angle (Θ) of
845 indicated lines, respectively. Bold horizontal lines indicate the median and whiskers
846 indicate the first and the third quarter of the data value. ***P<0.001; Student's *t*-test.

847 (F) Above (upper panels) and side (lower panels) views of indicated *M. polymorpha* lines.
848 Tak-1 (WT) expands its thallus horizontally on the agar surface. The overexpression of
849 MpPINZ-, AtPIN1-, and AtPIN2-GFP showed vertical thallus growth, which generated a
850 large angle between the lower surface of the thallus and the surface of the agar (Θ).
851 Scale bar = 0.5 cm.

852 (G) The quantification of the thallus growth angle (Θ) showed in A. Bold horizontal lines
853 indicate the median and whiskers indicate the first and the third quarter of the data

854 value. ***P<0.001; Student's *t*-test.

855 **Figure 4. Endogenous PINs present different localization patterns in different tissues.**

856 (A) The localization of PpPINA-GFP in tissues with different complexities. PpPINA-GFP is
857 polarized to the tip of initial and elongated protonema cells. The initial protonema cell
858 is regenerated from a detached leaf and the representative image shows the
859 maximum projection with a 5 µm thick Z-section. Auto-fluorescence of the
860 chloroplasts is indicated by asterisks. In elongated protonema cell, the polarity of
861 PpPINA-GFP is plotted by a intensity measurement along the PM as the yellow arrows
862 represented. The same measurement is applied to (B) and (C). In complex tissues
863 composed of multiple cell layers e.g. young leaves in *P. patens*, PpPINA-GFP is polarized
864 at both apical and basal domains (white arrowheads). Scale bars = 10 µm.

865 (B) The localization of MpPINZ-GFP in emerging rhizoids, young rhizoids, and gemma
866 epidermal cells. Representative image with a 5 µm thick Z-section at the gemma
867 surface shows the accumulation of MpPINZ-GFP at tips of emerging rhizoids as
868 indicated by yellow arrowheads in rhizoid precursor cells (asterisks). MpPINZ-GFP is
869 polarized at the tip of young rhizoids (middle). A middle section image showing the
870 even distribution of MpPINZ-GFP on the PM of gemmae composed of multiple cell
871 layers. Scale bars = 10 µm

872 (C) AtPIN2-GFP shows a polarized signal at the tip of the initial root hair but the
873 polarized signal is not observed in elongated root hairs. All imaging details are
874 described in Methods. The pixel values ranging from 0 to 255 are represented by the
875 rainbow color. In Arabidopsis epidermal cells, AtPIN2-GFP shows apical polarization as
876 white arrowheads indicated. Scale bar, 10 µm for root hairs, and 1 cm for epidermis.

877

878 **Figure 5. Xenologous PINs are PM localized with no defined polarity.**

879 (A) Overexpressed PpPINA-GFP is polarized to the tip of protonema, but overexpressed
880 AtPIN1-GFP is evenly distributed on the PM with intracellular puncta. The occurrence
881 frequency is indicated in the left lower corner in each image. Scale bars = 10 µm.

882 (B) Overexpressed MpPINZ-GFP is polarized to the tip of young rhizoids, while
883 overexpressed AtPIN1-GFP shows strong cytosolic signals and weak PM localization
884 with no polarity. Scale bars = 10 µm.

885 (C) AtPIN2-GFP under its native promoter is apicalized in epidermal cells, but PpPINA-

886 GFP and MpPINZ-GFP are mislocalized to the basal and lateral sites as white
887 arrowheads indicated. Scale bar = 1 cm.
888 (D) The intensity plots of the representative images for PpPINA-GFP, AtPIN1-GFP in *P.*
889 *patens* protonema cells and MpPINZ-GFP and AtPIN1-GFP in *M. polymorpha* young
890 rhizoids.
891 (E) Polarity index (ratio of signal intensity at the apical plasma membrane/ signal
892 intensity at the lateral plasma membrane) for apicalization of the indicated PIN-GFP
893 in Arabidopsis epidermal cells. PpPINA-GFP and MpPINZ-GFP are significantly lower
894 in the polarity index. 12-20 cells from 3 roots in three independent experiments for
895 each line. ***P<0.001; Student's *t*-test.
896
897 **Figure 6. Cytoskeletal networks are important for the polarization of mainly bryophytic PINs.**
898 (A) PpPINA-GFP is polarized to the tip of protonema, and the disruption of actin filaments
899 by Latrunculin (LatB) caused its hyperpolarization (white arrowhead). The disruption
900 of microtubules by Oryzalin (Ory) disturbed the polarization of PpPINA-GFP. Scale bars
901 = 10 µm.
902 (B) MpPINZ-GFP is polarized at the tip of young rhizoids, and its polarization was only
903 abolished by Oryzalin treatment (white arrowhead). Scale bars = 10 µm.
904 (C) AtPIN2-GFP is polarized at the apical site of epidermal cells, and disruption of either
905 actin filaments or microtubules did not change its polarization (white arrowheads).
906 Scale bars = 1 cm.
907 (D) Relative intensity of PpPINA-GFP and MpPINZ-GFP along the cell membrane with
908 indicated treatment.
909 (E) Polarity index of AtPIN2-GFP in indicated treatment, no significance is shown. The
910 concentration and duration of treatments for each species are described as in
911 Methods.
912
913
914

Figure 1. Phosphorylation sites are highly conserved between bryophytic and Arabidopsis PINs.

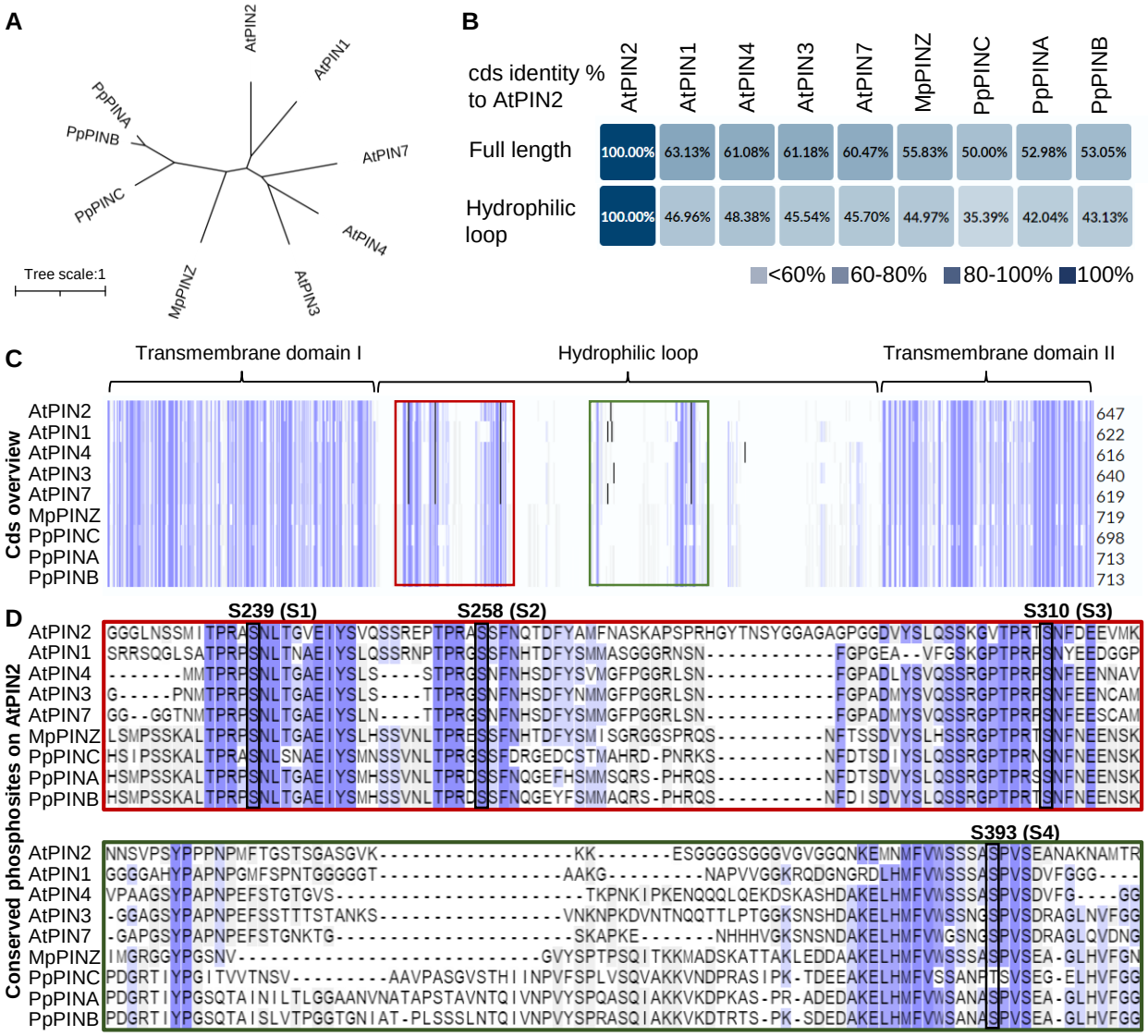

Figure 1. Phosphorylation sites are highly conserved between bryophytic and Arabidopsis PINs.

(A) Phylogenetic analysis of canonical PINs from early-divergent plants *P. patens (Pp), M. polymorpha (Mp),* and representative angiosperm *A. thaliana (At)*. The unrooted tree shows the relationships of different PINs in two representative bryophytes and Arabidopsis. The scale bar represents the number of changes per site.

(B) Identity indexes of all PINs compared to AtPIN2 with full length or only the hydrophilic loop region of coding amino acid sequences. Identity indexes of all PINs compared to AtPIN1 is shown in Supplemental Figure 1.

(C) Alignment of PIN amino acid sequences. Identical amino acids are highlighted with blue column. The rea and green boxes show the hydrophilic loop regions bearing conserved phosphorylation sites, which are enlarged in (D).

(D) Four conserved phosphorylation sites, labeled by S1 to S4, were verified in previous AtPIN2 studies and are depicted with black frames. Note that S1 to S4 are conserved in every examined PINs.

Figure 2. The hydrophilic loops in AtPIN2, PpPINA, and MpPINZ are less conserved.

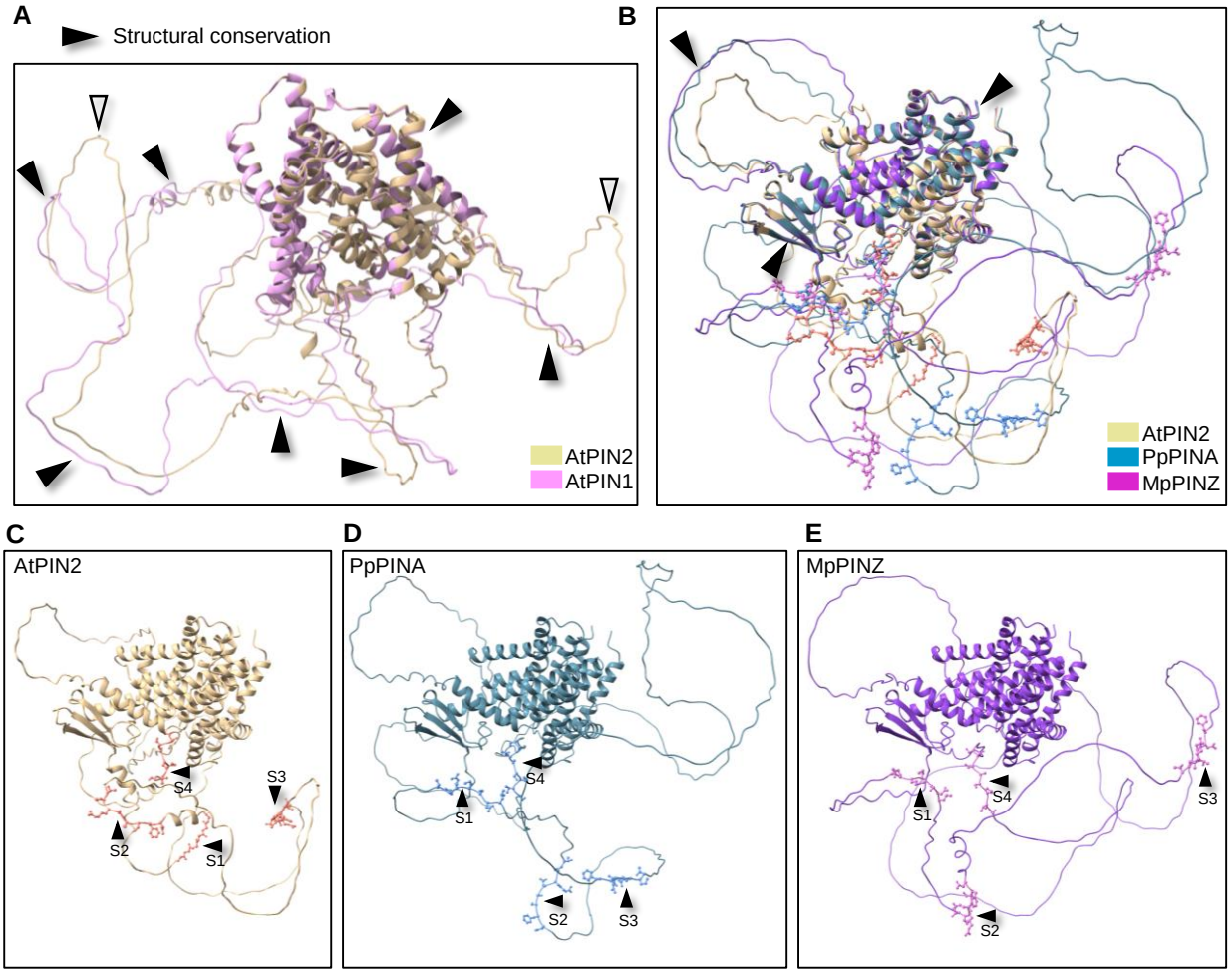

Figure 2. The hydrophilic loops in AtPIN2, PpPINA, and MpPINZ are less conserved.

(A) Structural alignment of AtPIN1 and AtPIN2. The protein structures are predicted by Alphafold2 and aligned in ChimeraX software. The structural conserved regions are indicated by black arrowheads, and the non-conserved regions are indicated by empty arrowheads.

(B) Structural alignment of AtPIN2 with PpPINA and MpPINZ. Only transmembrane domains and one loop aligned with each other, while the majority of hydrophilic loop regions are not conserved. The four conserved phosphorylation sites are labeled with atom details in ball-and-stick style.

(C) – (E) Individual protein structure retrieved from (B). The four conserved phosphorylation sites are indicated by arrowheads.

Figure 3. GFP-fused PIN proteins possess auxin export activity.

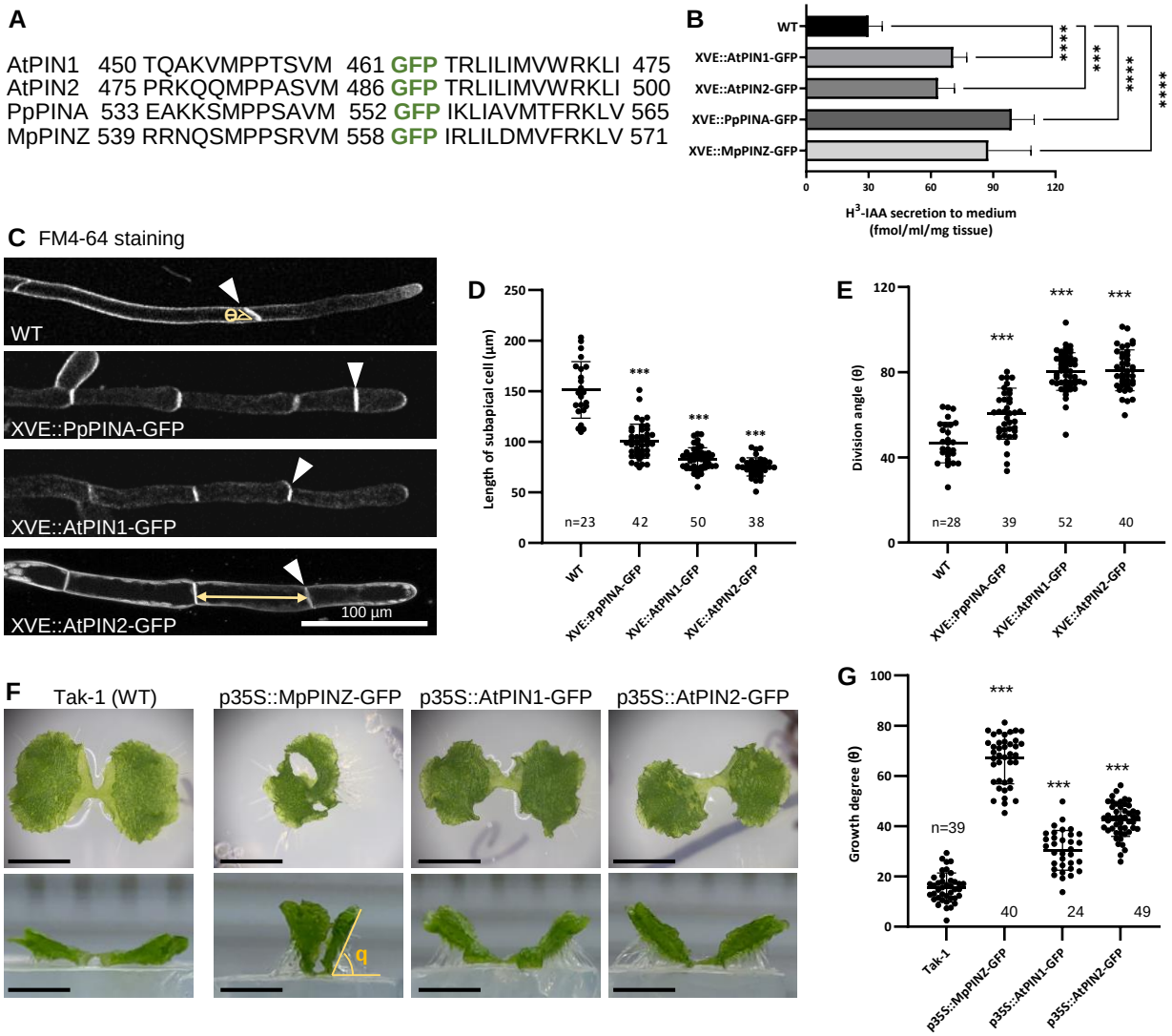

Figure 3. GFP-fused PIN proteins possess auxin export activity.

(A) The insertion site of GFP in indicated PIN proteins. Numbers represent the amino acid position in respective proteins.

(B) The auxin export assay with *P. patens* transgenic plants. Fresh tissues were incubated with radioactive H^3 IAA, followed by washing and the radiative H^3-IAA exported in the new culture medium was measured with the scintillation detector after one day.

(C) Representative protonema cells of the indicated genetic background. The cell outline was stained with FM4-64. White arrowheads indicate the first cell division plane, and the yellow double arrow indicates the cell length of the subapical cell. Scale bar = 100 µm.

(D) and (E), Quantitative results of the subapical cell length and the division angle (Θ) of indicated lines, respectively. Bold horizontal lines indicate the median and whiskers indicate the first and the third quarter of the data value. ***P<0.001; Student's *t*-test.

(F) Above (upper panels) and side (lower panels) views of indicated *M. polymorpha* lines. Tak-1 (WT) expands its thallus horizontally on the agar surface. The overexpression of MpPINZ-, AtPIN1-, and AtPIN2-GFP showed vertical thallus growth, which generated a large angle between the lower surface of the thallus and the surface of the agar (Θ). Scale bar = 0.5 cm.

(G) The quantification of the thallus growth angle (Θ) showed in A. Bold horizontal lines indicate the median and whiskers indicate the first and the third quarter of the data value. ***P<0.001; Student's *t*-test.

Figure 4. Endogenous PINs present different localization patterns in different tissues.

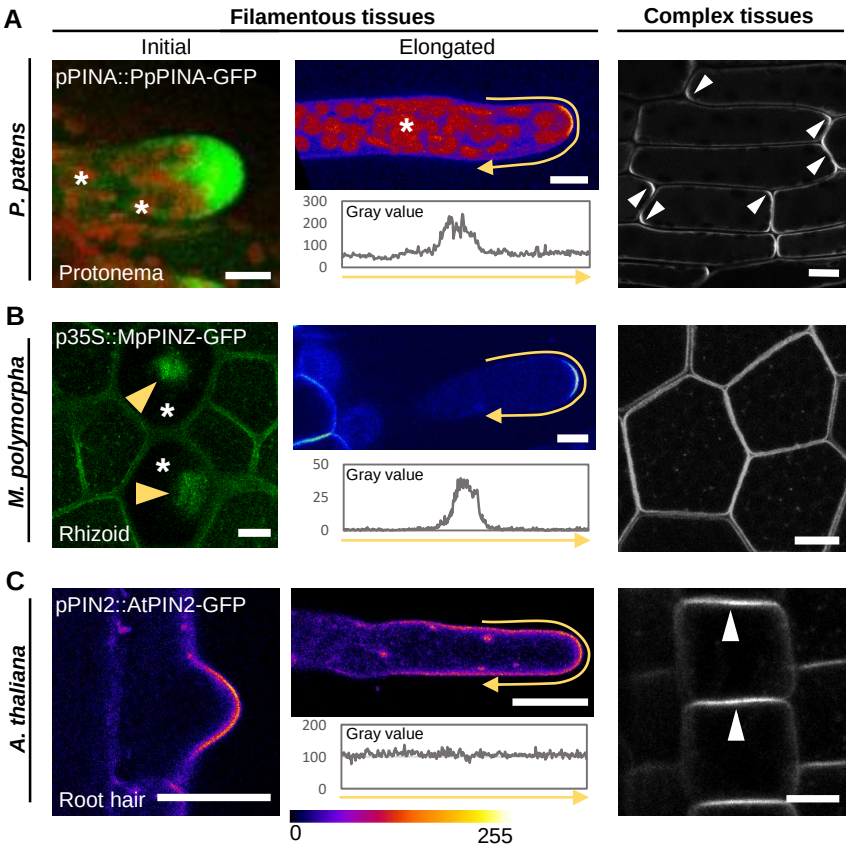

Figure 4. Endogenous PINs present different localization patterns in different tissues.

(A) The localization of PpPINA-GFP in tissues with different complexities. PpPINA-GFP is polarized to the tip of initial and elongated protonema cells. The initial protonema cell is regenerated from a detached leaf and the representative image shows the maximum projection with a 5 µm thick Z-section. Auto-fluorescence of the chloroplasts is indicated by asterisks. In elongated protonema cell, the polarity of PpPINA-GFP is plotted by a intensity measurement along the PM as the yellow arrows represented. The same measurement is applied to (B) and (C). In complex tissues composed of multiple cell layers e.g. young leaves in *P. patens*, PpPINA-GFP is polarized at both apical and basal domains (white arrowheads). Scale bars = 10 µm.

(B) The localization of MpPINZ-GFP in emerging rhizoids, young rhizoids, and gemma epidermal cells. Representative image with a 5 µm thick Z-section at the gemma surface shows the accumulation of MpPINZ-GFP at tips of emerging rhizoids as indicated by yellow arrowheads in rhizoid precursor cells (asterisks). MpPINZ-GFP is polarized at the tip of young rhizoids (middle). A middle section image showing the even distribution of MpPINZ-GFP on the PM of gemmae composed of multiple cell layers. Scale bars = 10 µm

(C) AtPIN2-GFP shows a polarized signal at the tip of the initial root hair but the polarized signal is not observed in elongated root hairs. All imaging details are described in Methods. The pixel values ranging from 0 to 255 are represented by the rainbow color. In Arabidopsis epidermal cells, AtPIN2-GFP shows apical polarization as white arrowheads indicated. Scale bar, 10 µm for root hairs, and 1 cm for epidermis.

Figure 5. Xenologous PINs are PM localized with no defined polarity.

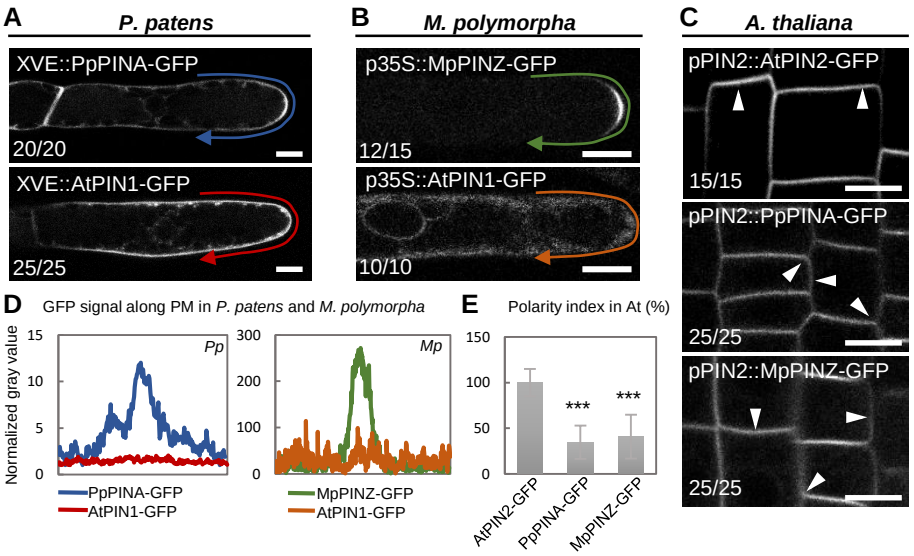

Figure 5. Xenologous PINs are PM localized with no defined polarity.

(A) Overexpressed PpPINA-GFP is polarized to the tip of protonema, but overexpressed AtPIN1-GFP is evenly distributed on the PM with intracellular puncta. The occurrence frequency is indicated in the left lower corner in each image. Scale bars = 10 µm.

(B) Overexpressed MpPINZ-GFP is polarized to the tip of young rhizoids, while overexpressed AtPIN1-GFP shows strong cytosolic signals and weak PM localization with no polarity. Scale bars = 10 µm.

(C) AtPIN2-GFP under its native promoter is apicalized in epidermal cells, but PpPINA-GFP and MpPINZ-GFP are mislocalized to the basal and lateral sites as white arrowheads indicated. Scale bar = 1 cm.

(D) The intensity plots of the representative images for PpPINA-GFP, AtPIN1-GFP in *P. patens* protonema cells and MpPINZ-GFP and AtPIN1-GFP in *M. polymorpha* young rhizoids.

(E) Polarity index (ratio of signal intensity at the apical plasma membrane/ signal intensity at the lateral plasma membrane) for apicalization of the indicated PIN-GFP in Arabidopsis epidermal cells. PpPINA-GFP and MpPINZ-GFP are significantly lower in the polarity index. 12-20 cells from 3 roots in three independent experiments for each line. ***P<0.001; Student's *t*-test.

Figure 6. Cytoskeletal networks are important for the polarization of mainly bryophytic PINs.

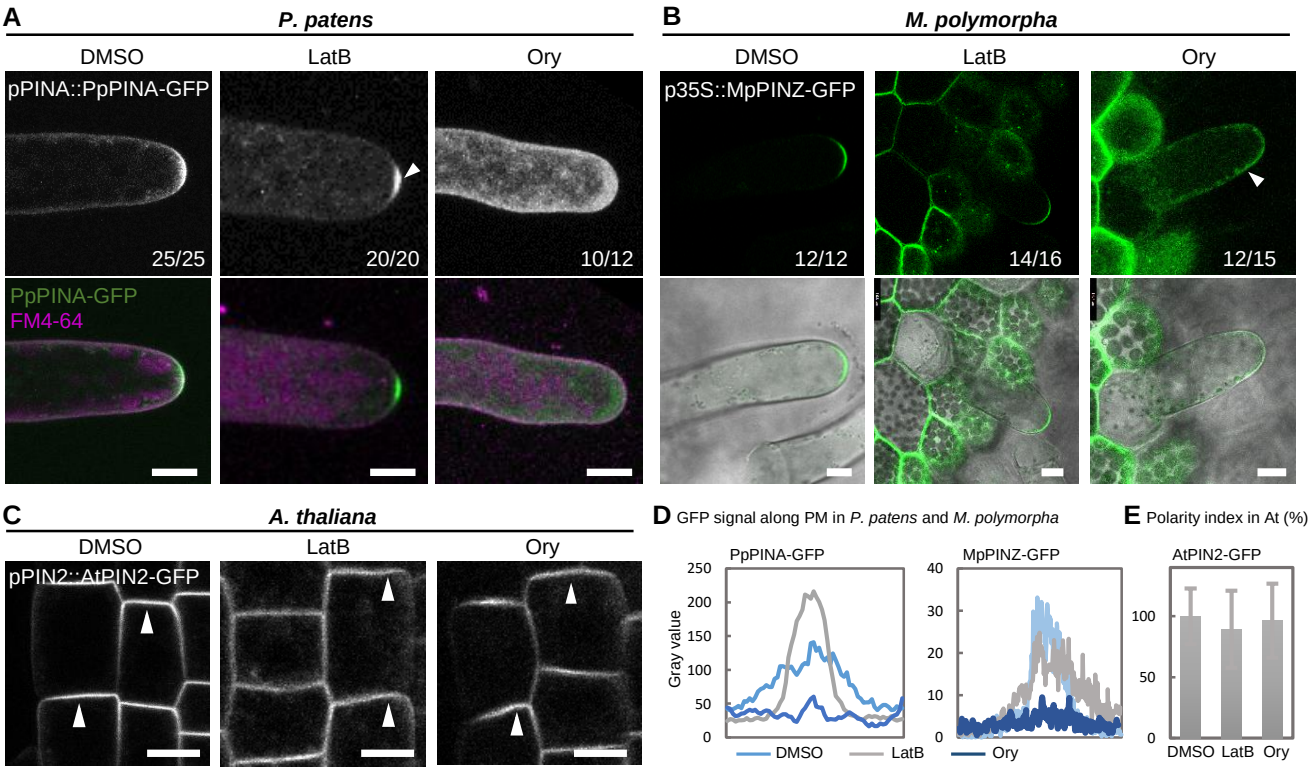

Figure 6. Cytoskeletal networks are important for the polarization of mainly bryophytic PINs.

(A) PpPINA-GFP is polarized to the tip of protonema, and the disruption of actin filaments by Latrunculin (LatB) caused its hyperpolarization (white arrowhead). The disruption of microtubules by Oryzalin (Ory) disturbed the polarization of PpPINA-GFP. Scale bars = 10 µm.
(B) MpPINZ-GFP is polarized at the tip of young rhizoids, and its polarization was only abolished by Oryzalin treatment (white arrowhead). Scale bars = 10 µm.
(C) AtPIN2-GFP is polarized at the apical site of epidermal cells, and disruption of either actin filaments or microtubules did not change its polarization (white arrowheads). Scale bars = 1 cm.
(D) Relative intensity of PpPINA-GFP and MpPINZ-GFP along the cell membrane with indicated treatment.
(E) Polarity index of AtPIN2-GFP in indicated treatment, no significance is shown. The concentration and duration of treatments for each species are described as in Methods.